nature communications

Article

https://doi.org/10.1038/s41467-024-53475-z

Water-promoted oxidative coupling of aromatics with subnanometer palladium clusters confined in zeolites

Received: 10 April 2024

Accepted: 11 October 2024

Published online: 30 October 2024

Check for updates

Yunchao Feng[1], Hongtao Wang[1], Tianxiang Chen[2], Miguel Lopez-Haro[3], Feng He[1], Zhe He[1], Carlo Marini[4], Benedict Tsz Woon Lo[2] & Lichen Liu[1]

A fundamental understanding of the active sites in working catalysts can guide the rational design of new catalysts with improved performances. In this work, we have followed the evolution of homogeneous and heterogeneous Pd catalysts under the reaction conditions for aerobic oxidative coupling of toluene for the production of 4,4′-bitolyl. We have found that subnanometer Pd clusters made with a few Pd atoms are the working active sites in both homogeneous and heterogeneous catalytic systems. Moreover, water can promote the activity of Pd clusters by nearly one-order magnitude for oxidative coupling reaction by facilitating the activation of O_2. These new insights lead to the preparation of a catalyst made with Pd clusters supported on a two-dimensional zeolite, which expands the scope of the oxidative coupling of aromatics to larger substrates.

The rational design of catalysts is one of the essential research topics in chemical engineering and catalysis sciences, which not only relies on atomic and molecular level understanding of the active sites and reaction mechanism but also relies on the precise construction of the catalysts with appropriate structural features[1]. Considering the dynamic structures of supported metal catalysts, the inter-transformations of metal entities among isolated metal atoms, clusters and nanoparticles can be associated with the activation and/or deactivation of the catalysts[2–5]. Following the structural evolution of the metal sites under reaction conditions will offer direct insights into the nature of the working active sites and guide the upgrading of the current systems rationally[6,7]. Typical examples of this research paradigm can be found in the works on the performance optimization of supported metal catalysts for gas-phase reactions, such as the dehydrogenation of light alkanes and hydrochlorination of acetylene as well as on the lifetime improvement of the catalysts for fluid catalytic cracking and methane combustion reaction[8–12].

In principle, metal catalysts will also undergo structural transformations in liquid-phase reactions, and probably in a more dramatic manner than the situation in gas-phase reactions, because of the strong interactions between metal species and solvent/ligands[13]. Though the advantages of solid catalysts in post-reaction separation and catalyst recycling are quite attractive to industrial processes, it is challenging to translate the above research paradigm into the rational design of solid catalysts for organic transformations, which could be hindered by difficulty in characterizing the structural features of metal active sites in liquid-phase systems[14,15].

In this work, we have attempted to tackle this challenge by studying the nature of the active sites in Pd-catalysed aerobic oxidative coupling of aromatics, which is an atom-economic route for sustainable production of biaryl compounds in comparison with other synthesis routes. Instead of using mononuclear Pd sites either in the form of molecular complex or immobilized Pd complex in zeolite (Fig. 1a)[16–18], we have developed a zeolite-confined Pd catalyst by incorporating subnanometer Pd clusters in the channels of Beta zeolite as an efficient catalyst for oxidative coupling of aromatics under acid-free conditions (Fig. 1b) through a different mechanism in comparison to the previously reported systems. One-order magnitude promotion in activity can be

[1]Department of Chemistry, Engineering Research Center of Advanced Rare Earth Materials, Tsinghua University, 100084 Beijing, China. [2]Department of Applied Biology and Chemical Technology, The Hong Kong Polytechnic University, 999077 Kowloon, Hong Kong, China. [3]Departamento de Ciencia de los Materiales e Ingeniería Metalúrgica y Química Inorgánica, Facultad de Ciencias, Universidad de Cádiz, Puerto Real 11510, Spain. [4]ALBA Synchrotron Light Source, Cerdanyola del Vallès, Barcelona 08290, Spain. e-mail: lichenliu@mail.tsinghua.edu.cn

https://doi.org/10.1038/s41467-024-53475-z

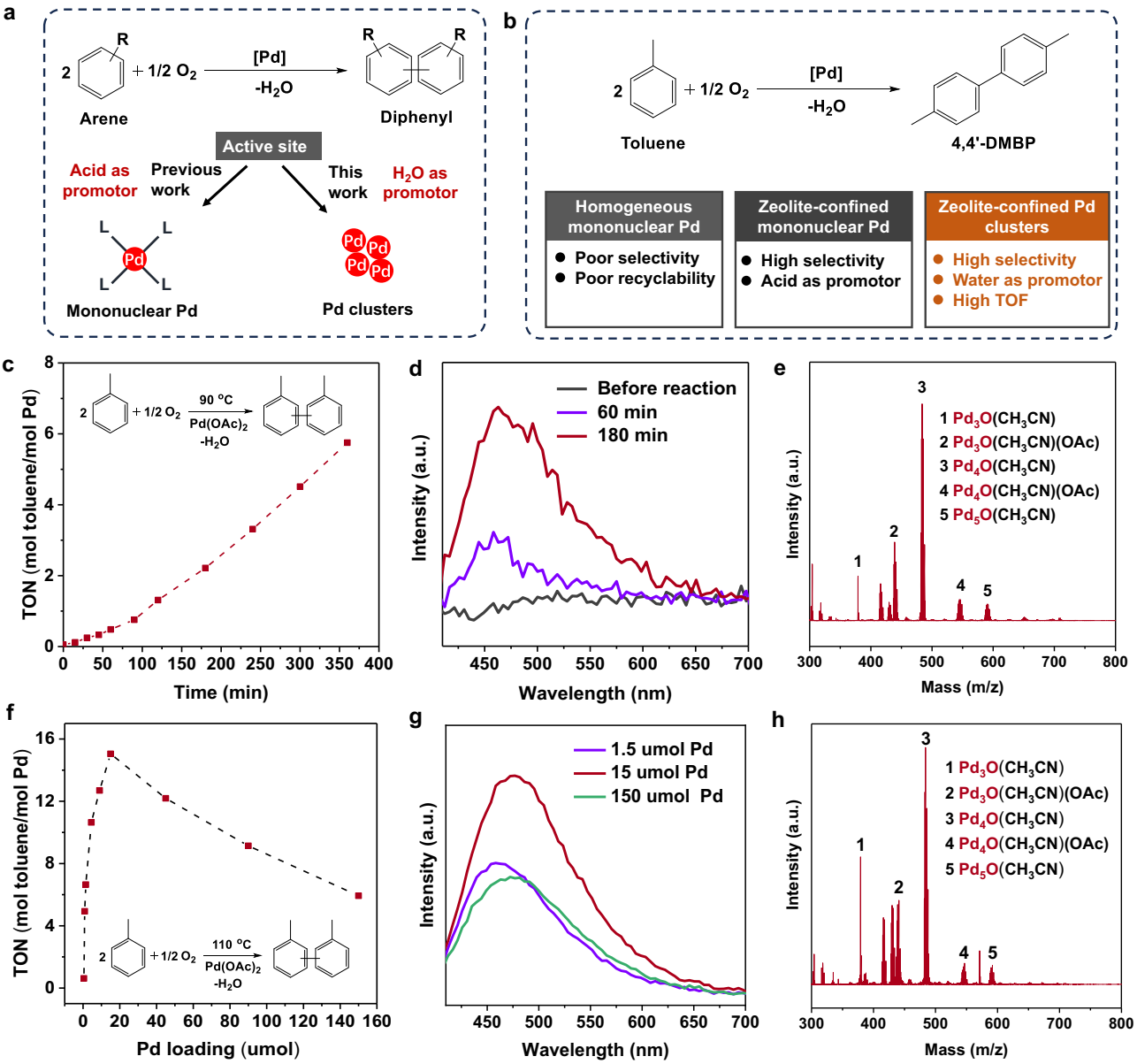

Fig. 1 | Oxidative coupling of toluene with homogeneous Pd catalyst. a and **b** Reaction schemes for oxidative coupling of arenes/toluene with homogeneous Pd catalyst and the proposed active species in the literature work and this work, respectively. **c** Kinetic profiles for the oxidative coupling of toluene with $Pd(OAc)_2$ as the starting catalyst. Reaction condition: toluene (4 mL), $Pd(OAc)_2$ (15 μmol), O_2 (16 bar), 90 °C and reaction time of 0–360 min. **d** Fluorescence emission spectra of the reaction mixture at different reaction times. **e** Analysis of the soluble Pd species in the reaction mixture after 180 min by mass spectrometry. A series of Pd clusters with different atomicity can be identified according to the *m*/*z* in the mass spectrum. **f** Turnover numbers for oxidative coupling of toluene obtained with different concentrations of $Pd(OAc)_2$ catalyst. Reaction condition: toluene (4 mL), $Pd(OAc)_2$ (0–15 μmol), O_2 (16 bar), 110 °C and reaction time of 140 min. **g** Fluorescence emission spectra of the reaction mixture of toluene coupling reaction catalysed by different concentrations of $Pd(OAc)_2$ complex. It should be noted that, when recording the fluorescence emission spectra, the reaction mixture is diluted to the same Pd concentration by toluene. **h** Analysis of the soluble Pd species in the reaction mixture by mass spectrometry.

achieved with H_2O by facilitating the activation of O_2 on the Pd clusters confined in the zeolite structure. Based on the structure–reactivity relationship established on the Pd/Beta zeolite catalyst, we have further developed a Pd/MWW zeolite catalyst made with Pd clusters supported on a two-dimensional zeolite with superior performances for activation of the challenging substrates, thus extending the catalyst and substrate scope for production of biaryl compounds with solid catalysts.

Results

Evolution of Pd catalyst in a homogeneous system

Initially, we studied the evolution behaviour of homogeneous Pd catalyst for oxidative coupling of toluene under acid-free conditions, which has been generally considered to be catalysed by mononuclear Pd sites[19]. As shown in Fig. 1c, an induction period of 60 min is observed in the kinetic profile for the toluene coupling reaction when using palladium acetate ($Pd(OAc)_2$) as the catalyst, implying that the starting Pd complex might not be the working active site. The fluorescence and mass spectroscopy characterizations of the reaction mixture at different reaction times indicate that partially oxidized Pd_{3-5} clusters are in situ formed in toluene (Fig. 1d, e)[20,21], which could serve as the working active species for oxidative coupling of toluene. This hypothesis is further supported by the experiments performed with different concentrations of $Pd(OAc)_2$ in toluene, in which an optimal initial reaction rate is achieved with a moderate concentration

https://doi.org/10.1038/s41467-024-53475-z

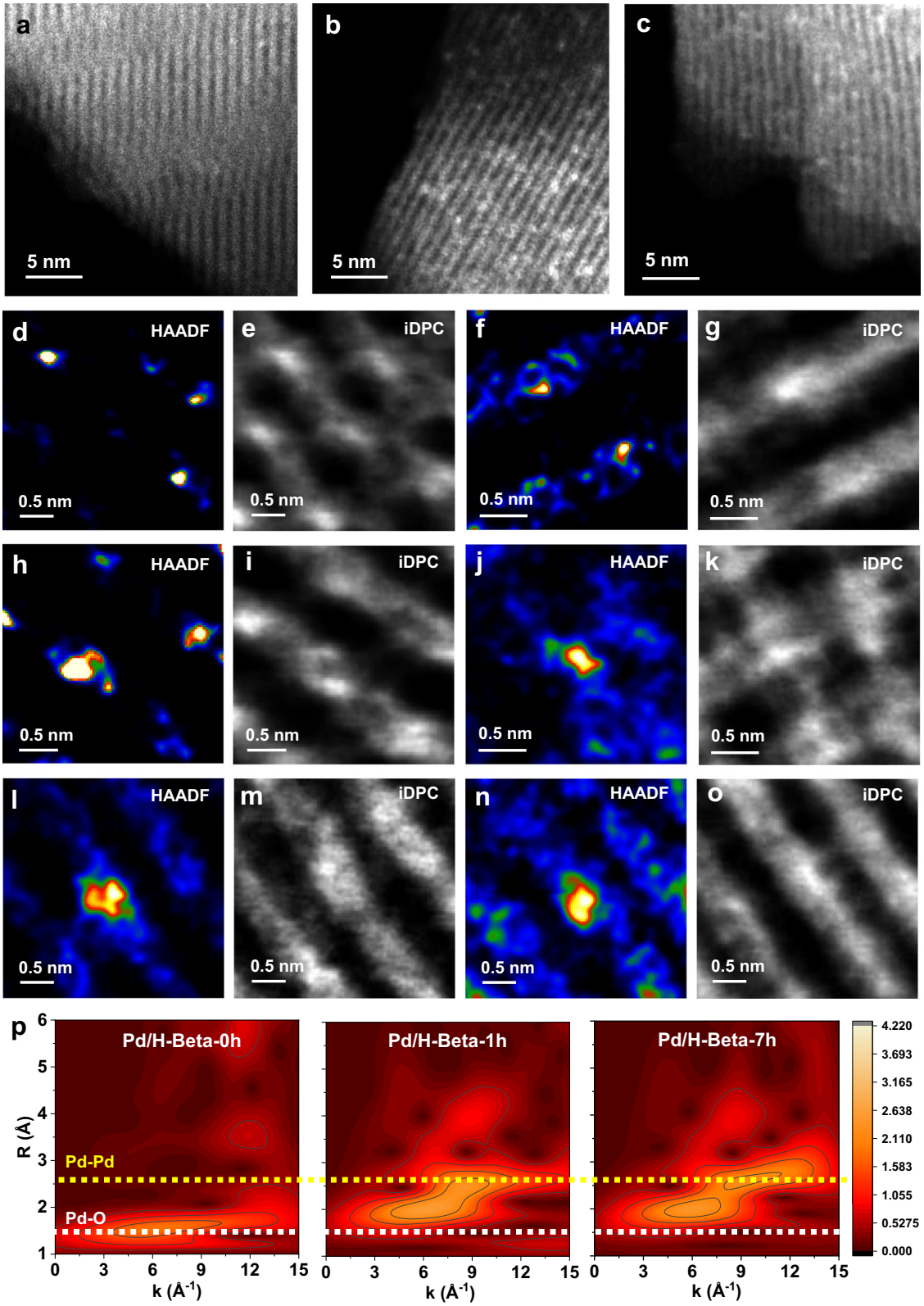

Fig. 2 | Structural characterizations of Pd/H-Beta catalyst along the reaction. **a**–**c** HAADF-STEM image of Pd/H-Beta zeolite catalysts isolated from the reaction mixture for oxidative coupling of toluene. **a** Pd/H-Beta-0h, **b** Pd/H-Beta-1h and **c** Pd/H-Beta-7h. In the Pd/H-Beta-0h sample, the Pd species are atomically dispersed within the Beta zeolite structure. In the Pd/H-Beta-1h and Pd/H-Beta-7h samples, subnanometer Pd clusters are observed as tiny bright particles in the HAADF-STEM images. **d**–**o** Determination of the location of subnanometer Pd species in the Beta zeolite structure by the combination of HAAD-STEM and iDPC-STEM imaging techniques. **d**–**g** Pd/H-Beta-0h, **h**–**k** Pd/H-Beta-1h and **l**–**o** Pd/H-Beta-7h. **p** Full-range Wavelet representation of the EXAFS spectra of the Pd/H-Beta catalyst isolated from the reaction mixture for oxidative coupling of toluene. Pd–O bonding is predominantly observed with the Pd/H-Beta-0h sample, while Pd–Pd bonding is also formed in the Pd/H-Beta-1h and Pd/H-Beta-7h sample.

https://doi.org/10.1038/s41467-024-53475-z

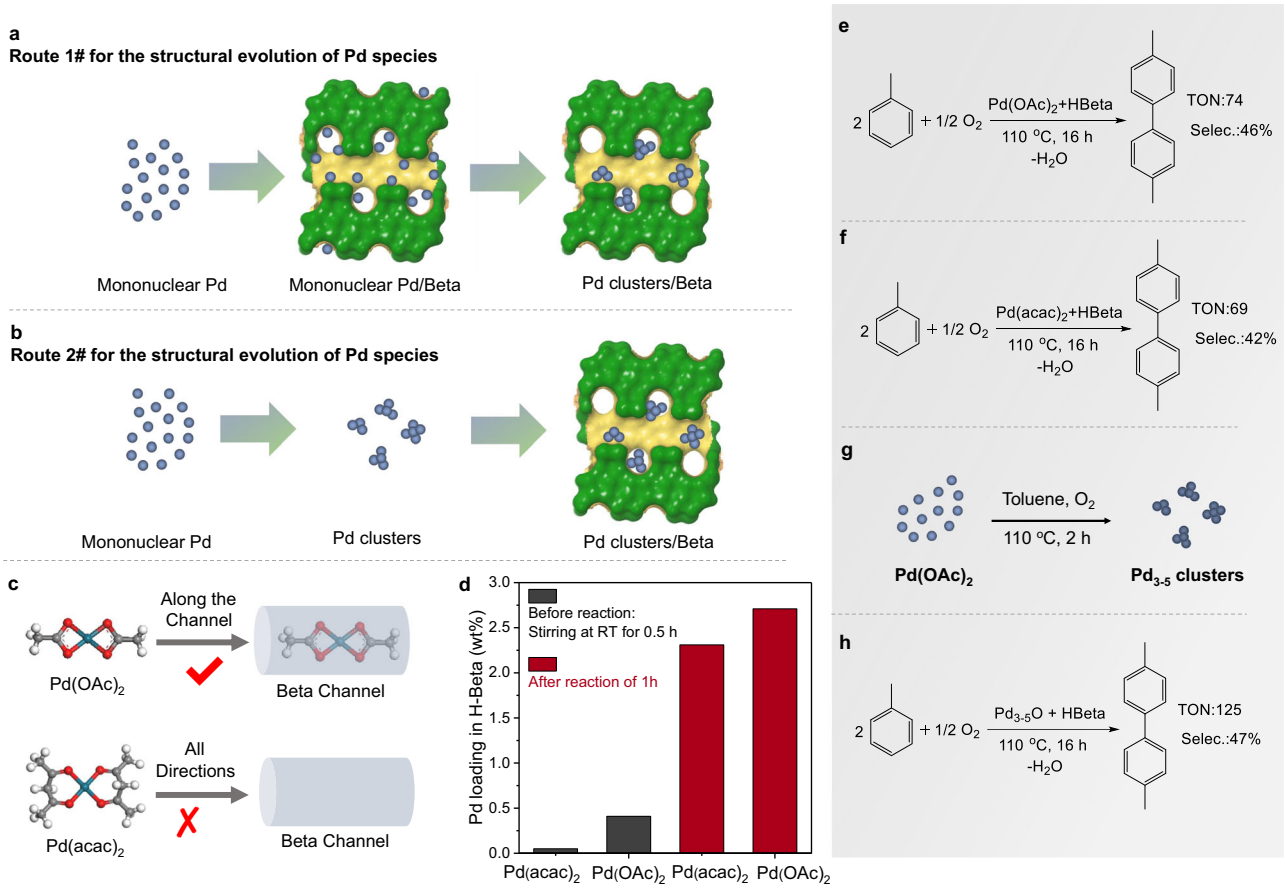

Fig. 3 | Structural evolution of Pd catalyst in Beta zeolite. a and **b** Two plausible routes of the formation of subnanometer Pd clusters in Beta zeolite from mononuclear Pd complex. In **Route 1**, the mononuclear Pd species enter into the zeolite microporous channels and then agglomerate into Pd clusters during the toluene coupling reaction. In **Route 2**, the mononuclear Pd complex transforms into Pd clusters, which further migrate into the microporous channels of Beta zeolite. The illustration of the Beta zeolite structure was created using the online tool provided by the Database of Disordered Zeolite Structures[32]. **c** Illustration of the molecular structure of $Pd(OAc)_2$ and $Pd(acac)_2$ in comparison with the pore dimension of Beta zeolite. **d** Pd contents in H-Beta zeolite when using $Pd(acac)_2$ and $Pd(OAc)_2$ as the starting catalyst. The Pd contents in the zeolite support isolated at the starting stage and after reaction for 1 h were analysed by ICP-OES. The Pd-zeolite samples isolated from the reaction mixture after 1 h contain much higher Pd loadings, indicating that the Pd clusters formed in the solution can be captured by Beta zeolite. **e**–**h** Comparison of the catalytic performances of Pd catalysts in heterogeneous systems. Turnover numbers of oxidative coupling of toluene by $Pd(acac)_2$, $Pd(OAc)_2$ and zeolite-confined $Pd_{3\text{-}5}$ clusters, respectively.

of Pd catalyst (Fig. 1f). The formation of partially oxidized Pd_{3-5} clusters is also observed under the optimal reaction conditions, as inferred by the fluorescence and mass spectra (Fig. 1g, h). The very low activity observed with highly diluted Pd catalyst could be caused by the unfavourable formation of Pd clusters, while the low activity observed with concentrated Pd catalyst could be ascribed to the growth of Pd species into the Pd nanoparticles, as observed in the characterization of the solid precipitate formed in the reaction mixture (Supplementary Fig. 1).

The agglomeration of molecular Pd complexes into Pd clusters has also been reported in other homogeneous systems, such as the Pd-catalysed C–X (X = C, N, S, etc.) cross-coupling and oxidative dehydrogenation reaction[3,21–23]. In our case, the formation of Pd clusters could be related to the decomposition of $Pd(OAc)_2$ in toluene accompanied by the partial reduction of Pd(II) into reduced Pd species[24,25]. Due to the absence of strongly coordinated ligands, the Pd clusters may continuously grow into clusters/particles with large sizes during extended reaction times (Supplementary Figs. 2, 3). Moreover, the in situ formation of Pd clusters as the active sites for aerobic coupling of toluene is also observed when using $Pd(acac)_2$ as the starting catalyst, and the similarity in the reaction performance of various Pd compounds could be associated with the formation of similar working active Pd species, which further infers the ubiquity of the dynamic transformation of molecular Pd catalysts (Supplementary Fig. 4). Considering the broad application of molecular Pd catalysts for organic oxidation reactions, it is of interest to study their potential structural transformations in other systems and identify the working active species by a variety of characterization techniques[22,26].

Evolution of Pd catalyst in a heterogeneous system

The results obtained in a homogeneous system encourage us to further investigate the evolution behaviour of Pd species in a heterogeneous system, in which Beta zeolite with 12MR channels (Supplementary Fig. 5) is introduced to accommodate Pd species to improve the regioselectivity to 4,4′-bitolyl in oxidative coupling of toluene (Supplementary Figs. 6–10)[17], because 4,4′-bitolyl is the precursor compound for the preparation of the monomers of biphenyl-type polyesters[27]. In the starting material, atomically dispersed Pd species are found in H-Beta zeolite, according to the experimental aberration-corrected HAADF-STEM images and the imaging simulation results (Fig. 2a, d–g and Supplementary Figs. 11–14). We have further tracked the morphologies of the Pd/H-Beta catalyst by characterizing the Pd/H-Beta catalysts isolated from the reaction mixture at different reaction times. The structural features of Pd species in Beta zeolite are further studied by correlating the paired images obtained in HAADF-STEM and integrated differential phase contrast (iDPC-STEM) imaging

mode, which allows us to identify the size and location of subnanometer Pd species in Beta zeolite structure[28]. The analysis of a set of HAADF-STEM and iDPC-STEM images indicates that Pd clusters of 0.4–0.7 nm are predominantly formed in the 12MR channels of Beta zeolite after reaction for 1 h (Fig. 2b, h–k, and Supplementary Figs. 15–19)[27]. Moreover, by analysing the Pd/H-Beta catalysts obtained after longer reaction times (1–7 h), we have found that the sizes of the Pd clusters remain almost unchanged, inferring the stabilization effect of the 12MR channels of Beta zeolite on the Pd clusters (Fig. 2c, i–o, Supplementary Figs. 20–25). After reaction for 10 h, the vast majority of the Pd species exist as subnanometer Pd clusters within the 12MR channels of Beta zeolite together with quite a few Pd nanoparticles of 1–2 nm, suggesting the continuous evolution of Pd species under the reaction conditions (Supplementary Fig. 26). By correlating the kinetic profile and the size distributions of Pd species in H-Beta zeolite, we tentatively conclude that the Pd clusters formed in H-Beta zeolite could be the working active sites while the agglomeration of Pd clusters into Pd nanoparticles may cause the deactivation of the catalyst.

The structural transformation of Pd species in H-Beta zeolite under reaction conditions is further studied by X-ray absorption spectroscopy. As shown in Fig. 2p, in the starting Pd/H-Beta catalyst, Pd–O bonding is predominantly observed in the Pd K-edge extended X-ray absorption fine structure (EXAFS) spectra, which is consistent with the formation of mononuclear Pd species in H-Beta zeolite by HAADF-STEM. The formation of Pd–Pd bonding is confirmed by the wavelet transformations of Pd K-edge EXAFS spectra of the spent catalysts, suggesting the agglomeration of mononuclear Pd species into subnanometer Pd clusters under reaction conditions[29,30]. The fitting results of the EXAFS spectra show that the average atomicity of the Pd clusters should be <10 and probably be in the range of 3–8, which is well in line with the electron microscopy images (Supplementary Table 1). The formation of subnanometer Pd clusters on Beta zeolite is consistent with the XRD patterns and XPS spectra (Supplementary Figs. 27, 28) of the spent catalysts[31].

The observation of Pd clusters in the working Pd/H-Beta catalyst encourages us to further clarify the formation mechanism of Pd clusters from the $Pd(OAc)_2$ precursor. As illustrated in Fig. 3a, one possible route is the adsorption, migration, and agglomeration of mononuclear Pd species within the micropores of Beta zeolite[32]. However, considering the very close molecular size of $Pd(OAc)_2$ to the 12MR channels of Beta zeolite, the diffusion of $Pd(OAc)_2$ along the 12MR channels of Beta zeolite is not favourable. Besides, we have also tested other Pd compounds, which also show catalytic activities for oxidative coupling of toluene (Fig. 3e, f). For instance, $Pd(acac)_2$ exhibits a larger molecular size than the 12MR channels of Beta zeolite (Fig. 3c and Supplementary Fig. 29), and it cannot be adsorbed by Beta zeolite at room temperature according to the composition analysis results in Fig. 3d, inferring the formation of Pd clusters may proceed in another route (Fig. 3b), in which the Pd precursors are transformed into subnanometer Pd clusters with a few atoms in toluene and then captured and stabilized by Beta zeolite. This hypothesis is confirmed by the control experiments in which Pd clusters are generated from the decomposition of $Pd(OAc)_2$ in toluene and then immobilized into Beta zeolite for catalysing the oxidative coupling reaction (Fig. 3g, h).

Modifying the catalytic properties by alkali metals

Considering the promotive role of alkali metals in various metal-zeolite catalysts, we have tested the catalytic performances of a series of Pd/Na-Beta catalysts prepared by exchanging the H^+ in H-Beta zeolite with different Na contents, as implied by the measurements of the Brønsted acid sites by pyridine-IR spectroscopy (Supplementary Fig. 30)[33–36]. The performances of the Pd/Beta catalysts are expressed by the turnover numbers (TON) obtained at low conversion levels to show the intrinsic activities of the Pd species in different catalysts (see the correlation of TON and toluene conversion in Supplementary Fig. 31). As shown in Fig. 4a and Supplementary Fig. 32, partial exchange of H^+ into Na^+ (corresponding to the Pd/29Na-Beta sample) will cause a sharply increased activity in oxidative coupling of toluene while higher exchange degrees will cause declined performances. Nevertheless, a higher degree of exchange of H^+ by Na^+ (the Pd/51Na-Beta sample) still leads to better performance than the pristine Pd/H-Beta catalyst.

Moreover, we have followed the kinetic profiles of three representative Pd/Beta catalysts to understand the impacts of Na^+ on the catalytic properties (Fig. 4b, Supplementary Figs. 6 and 33, 34). At the starting stage (0–3 h), the three Pd/Beta catalysts exhibit very similar behaviour, but marked differences are observed after 3 h. During the reaction period of 3–10 h, the Pd/H-Beta catalyst exhibits a gradual deactivation pattern while dramatically promoted reaction rates are observed with Pd/29Na-Beta and Pd/51Na-Beta. In particular, the Pd/29Na-Beta sample exhibits a 2-fold reaction rate of Pd/51Na-Beta and a 15-fold reaction rate of Pd/H-Beta (Fig. 4c), suggesting the importance of precise control of the exchange degree of H^+ by Na^+.

We have tracked the structural transformations of Pd species in Na-modified Pd/Beta catalysts during the oxidative coupling of toluene. As shown in Fig. 4d–s and Supplementary Figs. 35–58, mononuclear Pd species are present in the starting catalysts and then transform into subnanometer Pd clusters confined in the 12MR channels of Beta zeolite under reaction conditions, showing very similar evolution behaviour as the Pd/H-Beta catalyst. The evolution behaviours of mononuclear Pd clusters on Na-modified Beta zeolite are also studied by Pd K-edge EXAFS spectra, in which the formation of Pd–Pd bonding is observed (Fig. 4t, Supplementary Fig. 59 and Supplementary Table 2). The essential role of subnanometer Pd clusters as the active sites in the Na-modified Pd/Beta catalysts is further validated by the catalytic tests of Pd/29Na-Beta catalysts with different Pd loadings (Supplementary Fig. 54). At low Pd loading, the Pd species predominantly exist as atomically dispersed Pd species on Beta zeolite, resulting in low activities. When the Pd loading surpasses a threshold, a large number of Pd clusters are formed in 29Na-Beta zeolite, resulting in high activities (Supplementary Figs. 60–66).

By carefully analysing the particle size and location of the Pd clusters in the spent Pd/H-Beta and Na-modified Pd/Beta catalysts by electron microscopy imaging technique, we have not found marked differences in their structural features, despite their very large discrepancies in activity. These results indicate that the distinct catalytic properties of various Pd/Beta catalysts could be associated with subtle differences in structural features of the active sites (e.g. microenvironment of the Pd species, the absorbates on the active sites, etc.), which could not be directly visualized/probed by the conventional spectroscopy (Supplementary Fig. 67) and electron microscopy technique.

Influence of H_2O on the catalytic behaviour of Pd clusters

In Pd-catalysed oxidation reactions, water can show profound impacts on the activity and stability of the supported Pd catalysts[37–39]. Regarding the reaction system studied in this work, it has been proposed that the H_2O produced in the oxidative coupling of toluene can block zeolite pores/channels, thus leading to the gradual deactivation of the Pd/H-Beta catalyst[17,40]. Indeed, the replacement of H^+ with Na^+ can indeed improve the hydrophobicity of Beta zeolite as suggested by the adsorption properties for H_2O (Fig. 5a). With a higher degree of exchanging H^+ with Na^+, a lower adsorption capacity of H_2O is observed. Considering the structural features of the Pd/Beta catalysts and the reaction mechanism, the prominent impacts of Na^+ on the catalytic performances could be associated with the physicochemical properties of H_2O in different Pd/Beta catalysts and the interaction between H_2O and the Pd active sites.

To further verify the above hypothesis, we have systematically studied the influence of H_2O amount on the catalytic performances of different Pd/Beta catalysts. As shown in Supplementary Fig. 68a, when

https://doi.org/10.1038/s41467-024-53475-z

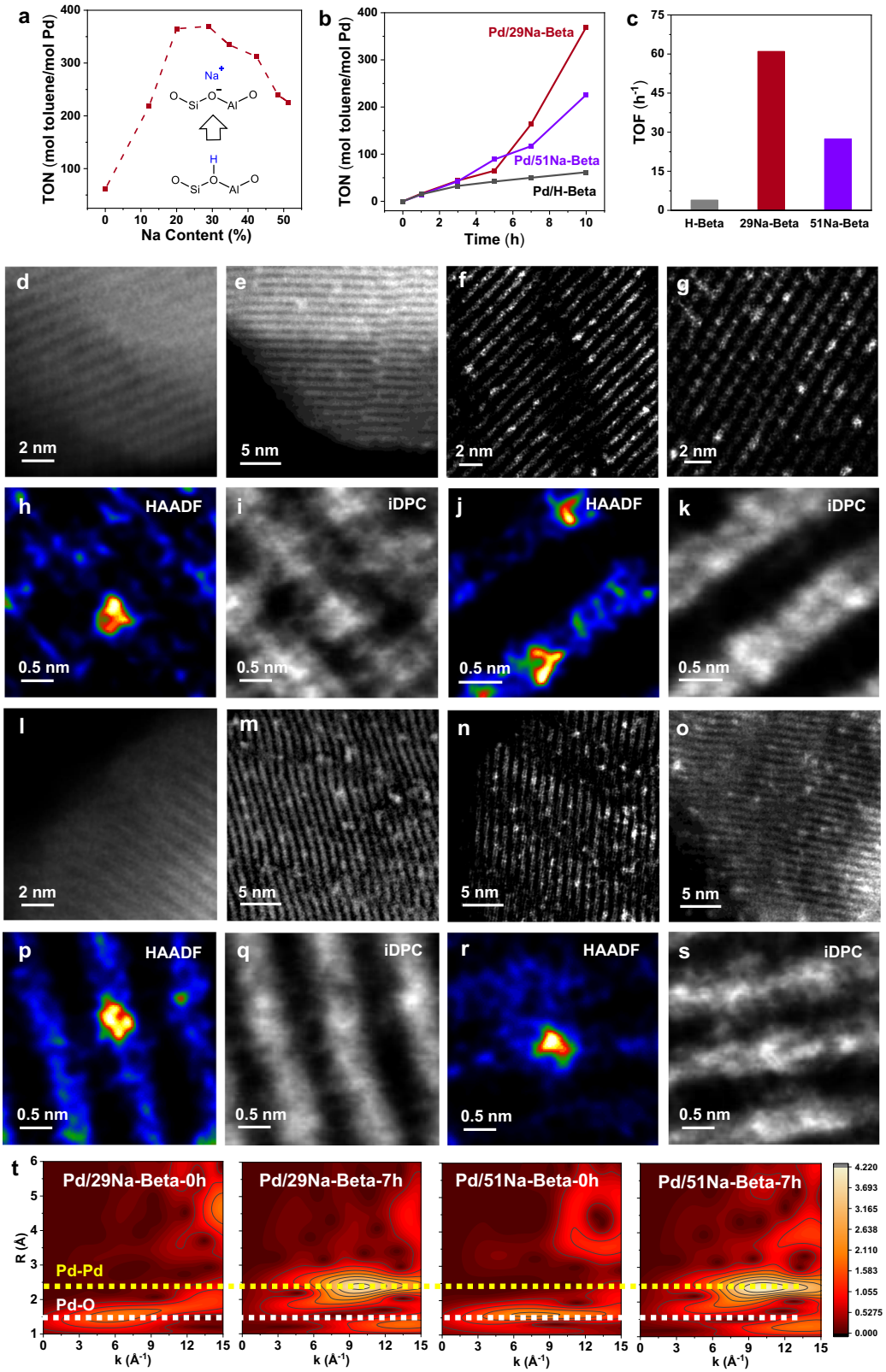

using 29Na-Beta as the support for Pd species, the induction period can be greatly shortened from 7 to <1 h, and a high turnover number (TON) for oxidative coupling of toluene can be achieved by adding a very small amount of H_2O (10 μL) into the reaction medium. The imperative involvement of H_2O in the Pd/Beta catalyst is proven by a set of control experiments (Supplementary Fig. 68b), in which the addition of water absorbent (anhydrous $MgSO_4$ and small-pore zeolite) will result in the loss of activity for the toluene coupling reaction. The amount of water promotor has marked impacts on the structural features of the Pd species formed on 29Na-Beta because an excess amount of water will cause the agglomeration of Pd species on the external surface of 29Na-Beta zeolite due to the formation of mobile $Pd(OH)_x$ species[41], resulting in low activities (Supplementary Figs. 69, 70).

https://doi.org/10.1038/s41467-024-53475-z

Fig. 4 | Modifying the catalytic properties by alkali metals. a Influence of the Na content in the Na-exchanged Beta zeolite on the catalytic performance for oxidative coupling of toluene. **b** Kinetic profiles of the three Pd/Beta zeolite catalysts for oxidative coupling of toluene, which indicates the presence of an induction period of 5 and 3 h for the Pd/29Na-Beta and Pd/51Na-Beta catalyst, respectively. **c** Turnover frequencies of the three Pd/Beta catalysts for oxidative coupling of toluene during the reaction period of 5–10 h. **d**–**g** HAADF-STEM images of Pd/29Na-Beta catalyst isolated from the reaction mixture at different times. **d** Pd/29Na-Beta-0h, **e** Pd/29Na-Beta-1h, **f** Pd/29Na-Beta-5h and **g** Pd/29Na-Beta-7h. **h**–**k** Determination of the location of subnanometer Pd clusters in the Pd/29Na-Beta-1 h (**h**, **i**) and Pd/29Na-Beta-7 h (**j**, **k**) by HAADF-STEM and iDPC-STEM imaging technique. **l**–**o** HAADF-STEM images of Pd/51Na-Beta catalyst isolated from the reaction mixture at different times. **l** Pd/51Na-Beta-0h, **m** Pd/51Na-Beta-1h, **n** Pd/51Na-Beta-5h and **o** Pd/51Na-Beta-7h. **p**–**s** Determination of the location of subnanometer Pd clusters in the Pd/51Na-Beta-1h (**p**, **q**) and Pd/51Na-Beta-7h (**r**, **s**) by HAADF-STEM and iDPC-STEM imaging technique. **t** Full-range Wavelet representation of the EXAFS spectra of the Pd/29Na-Beta and Pd/51Na-Beta catalyst isolated from the reaction mixture for oxidative coupling of toluene. Pd–O bonding is predominantly observed with the starting Pd/29Na-Beta-0h and Pd/51Na-Beta-0h sample, while Pd–Pd bonding is also formed in the catalysts after the reaction.

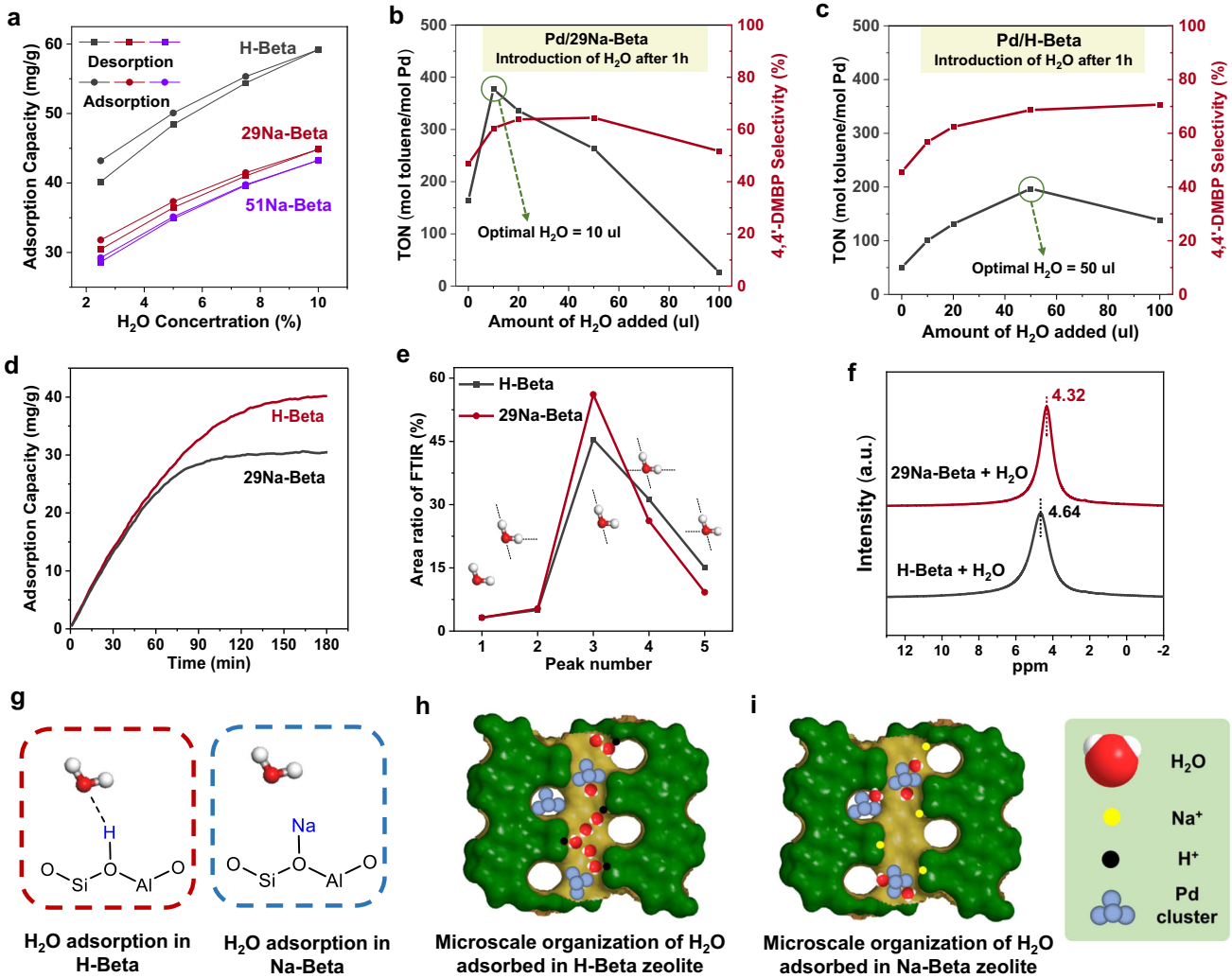

Fig. 5 | Influence of H_2O on the catalytic performance of Pd clusters. a The water vapour adsorption-desorption capacities of H-Beta, 29Na-Beta and 51Na-Beta at 25 °C. **b** and **c** Influence of the water promotor on the catalytic performance of Pd/29Na-Beta-1h and Pd/H-Beta-1h catalyst. Different amounts of H_2O were added to the reaction mixture after 1 h. Reaction condition: toluene (4 mL), Pd/29Na-Beta-1h or Pd/H-Beta-1h, O_2 (16 bar), 110 °C, 6 h. **d** Amount of H_2O produced from the toluene coupling reaction after the reaction of 5 h. **e** Hydrogen bond interaction of H_2O in H-Beta and 29Na-Beta zeolites obtained from FTIR. **f** ^1H MAS NMR spectra of H_2O loading on the H-Beta and 29Na-Beta zeolite. **g** Illustration of the interaction between water molecules and the H-Beta and 29Na-Beta zeolite framework. The illustration of the Beta zeolite structure was created using the online tool provided by the Database of Disordered Zeolite Structures[32]. **h**, **i** Illustration of the microscale organization of water molecules adsorbed in H-Beta and Na-Beta zeolite. In the case of H-Beta, more water molecules will be adsorbed into the channels of H-Beta zeolite and the water molecules tend to form water clusters via hydrogen bonding interaction. In the case of Na-Beta, fewer water molecules will be adsorbed into the channels of Na-Beta zeolite and the water molecules tend to be adsorbed on Pd clusters.

Further control experiments by adding water after the formation of Pd clusters in the 29Na-Beta zeolite show that the major influence of the water promotor is very likely to be associated with the interaction of H_2O and Pd clusters rather than with the formation of Pd clusters (Fig. 5b and Supplementary Figs. 71–75). In the case of H-Beta, a considerably higher amount of H_2O (50 µL) is required to achieve the optimum activity (Fig. 5c and Supplementary Figs. 76–80). Because the H-Beta zeolite has a higher adsorption capacity for H_2O due to its higher level of hydrophilicity than the Na-modified Beta, a relatively high amount of H_2O is required to ensure the formation of intimate

https://doi.org/10.1038/s41467-024-53475-z

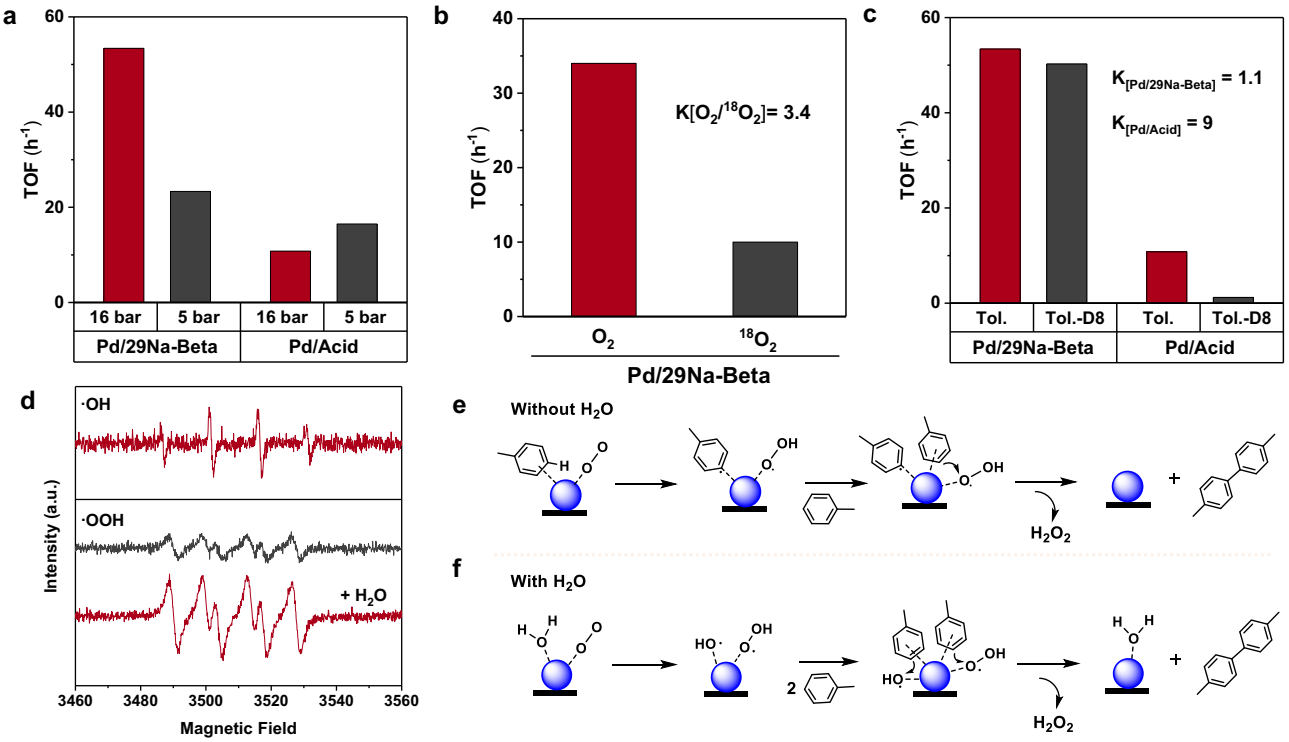

Fig. 6 | Mechanistic study of the zeolite-confined Pd clusters. a Effect of O_2 pressure on TOF values. Reaction condition: toluene (4 mL), $Pd(OAc)_2$ (15 μmol), O_2 (5 bar/16 bar), 110 °C, 0–7 h, 29Na-Beta (50 mg), H_2O (10 μL) for Pd/29Na-Beta system and acetic acid (200 μL) for Pd/Acid system. **b** Kinetic isotope effects (KIE) of $O_2/^{18}O_2$ obtained from TOF. Reaction condition: toluene (1 mL), $Pd(OAc)_2$ (3.75 μmol), 29Na-Beta (12.5 mg), $O_2/^{18}O_2$ (5 bar), 110 °C, 0–7 h. **c** Kinetic isotope effects (KIE) of Toluene-D8/Toluene obtained from TOF. Reaction condition: toluene/toluene-D8 (4 mL), $Pd(OAc)_2$ (15 μmol), 29Na-Beta (50 mg), H_2O (10 μL), O_2 (16 bar), 110 °C, 0–7 h. **d** EPR spectra of ·OOH and ·OH radicals. **e** and **f** Proposed reaction mechanism for the oxidative coupling of toluene on Pd active sites in the absence and presence of H_2O.

interaction between Pd clusters and H_2O molecules within the Beta zeolite channels (Fig. 5d). In the case of Na-modified Beta, due to the low affinity of H_2O to the zeolite framework, the H_2O molecules within the zeolite channels are preferentially adsorbed by the Pd clusters instead of by the zeolite framework. Consequently, it is sufficient to achieve a remarkable promotion effect by adding a small of H_2O into the reaction mixture.

Moreover, the maximum activity achieved with the Pd/H-Beta is only half of that obtained with the Pd/29Na-Beta catalyst (Fig. 5b, c) though the Pd clusters formed in the H_2O-promoted Pd/H-Beta and Pd/29Na-Beta catalyst show similar size distributions, number of the Pd clusters in Beta zeolite supports and their locations within the Beta zeolite channel systems (Supplementary Figs. 81–84). These results imply that besides the adsorption capacity for H_2O, the physicochemical properties of H_2O could be affected by the Na^+ added into Beta zeolite. This point is also implied by the similar reaction rates of the different Pd/Beta catalysts during the induction period (0–3 h) and their distinct behaviours after the induction period (3–10 h). We have characterized the topological features of water molecules in Beta zeolites by IR spectroscopy (Fig. 5e and Supplementary Fig. 85), indicating that fewer hydrogen bonding interactions between the H_2O molecules are likely present with the 29Na-Beta zeolite sample[42]. The influence of Na^+ on the physicochemical properties of H_2O confined in Beta zeolite is also supported by the lower shift of the 29Na-Beta sample in the ^{1}H-NMR spectra (Fig. 5f)[43,44]. Due to the replacement of H^+ with Na^+, the interaction between the confined H_2O molecules and the Beta zeolite framework is probably weakened (Fig. 5g), resulting in the local enrichment of H_2O on Pd clusters in the Pd/29Na-Beta sample as illustrated in Fig. 5h, i[45].

The above discussion can further be extended to the interpretation of the declined activity observed with the Pd/51Na-Beta sample. With a more hydrophobic environment inside the 51Na-Beta zeolite, a more intimate contact between H_2O molecules and Pd clusters is formed, which will aggravate the sintering of Pd species even at low H_2O concentration levels. Indeed, as shown in the electron microscopy images, the particle sizes of the Pd clusters are slightly larger in the Pd/51Na-Beta-7h than the samples with lower Na contents (Fig. 4p–s and Supplementary Fig. 57), though a considerable amount of sub-nanometer Pd clusters are also observed within the Pd/51Na-Beta-7h sample.

As shown in Fig. 5b, c, with the same amount of H_2O promotor (50 μL), the Pd/H-Beta sample gives almost the same selectivity (~68%) to 4,4′-bitolyl as the Pd/29Na-Beta sample (~65%). The regioselectivity to 4,4′-bitolyl is mainly controlled by the pore dimension of the 12MR channel of Beta zeolite. The shape selectivity induced by the Beta zeolite framework causes the formation of 4,4′-bitolyl as the major product because the molecular sizes of other isomer products are larger than the pore dimension of the 12MR channels.

Mechanistic study of the zeolite-confined Pd clusters

To understand the reaction mechanism of Pd clusters, we have carried out kinetic and isotopic studies to reveal the rate-determining step in the oxidative coupling of toluene. As shown in Fig. 6a–c, by increasing the O_2 partial pressure from 5 to 16 bar, the initial reaction rate of toluene increases accordingly, suggesting that O_2 activation could be a key step in the oxidative coupling reaction. Furthermore, when using D_8-toluene as the reactant, we can only observe a minor kinetic isotopic effect of ~1 (KIE), implying that the C–H activation might not be the rate-determining step. We have also studied the catalytic behaviour of traditional molecular Pd catalysts under the same conditions. The results indicate that the homogeneous Pd catalyst exhibits a profound KIE of ~9 while the initial reaction rate is not sensitive to O_2

https://doi.org/10.1038/s41467-024-53475-z

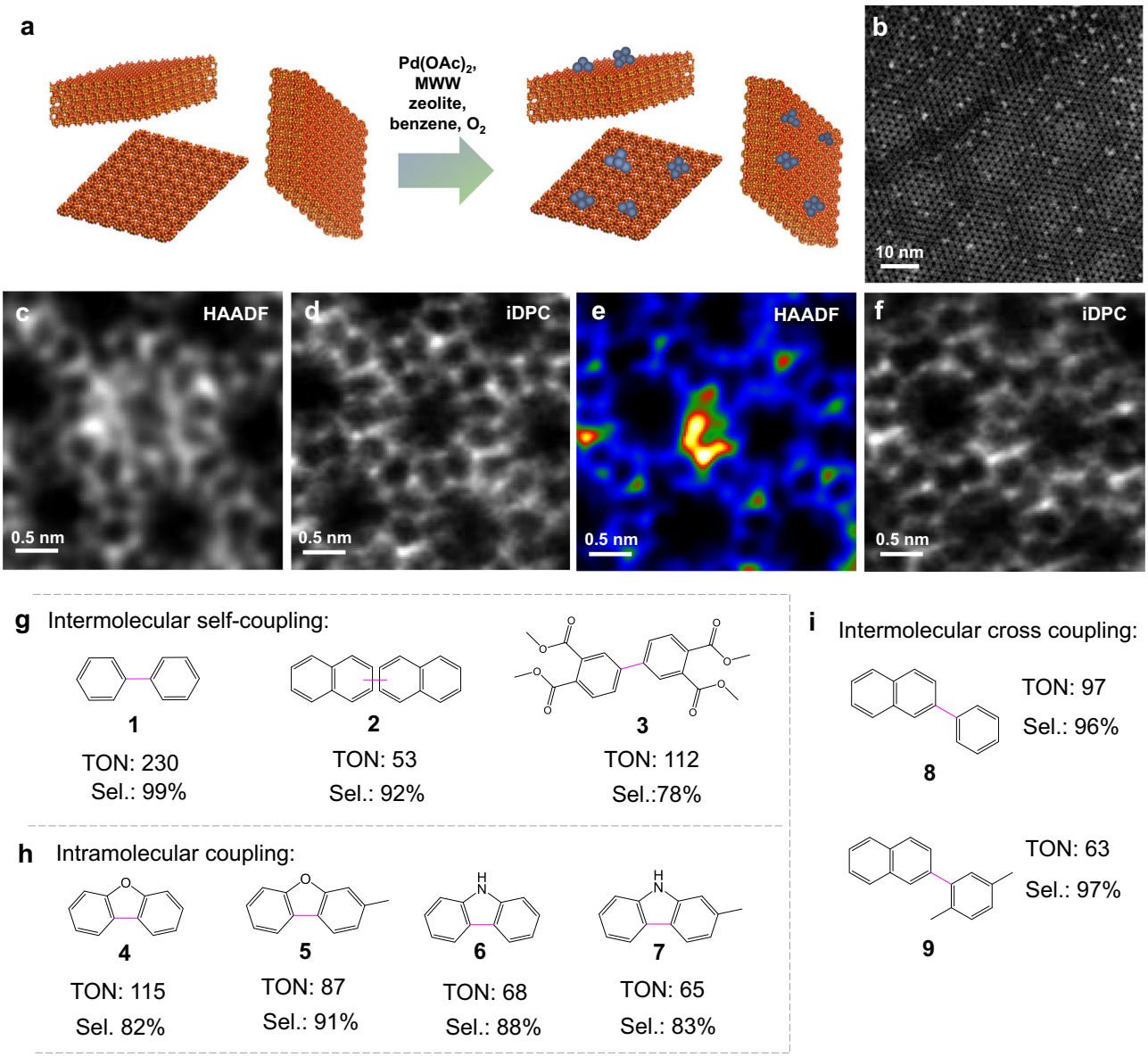

Fig. 7 | Oxidative coupling of arenes with Pd/MWW catalyst. a Illustration of the formation of subnanometer Pd clusters on an MWW-type zeolite support with two-dimensional morphology. The illustration of the Beta zeolite structure was created using the online tool provided by the Database of Disordered Zeolite Structures[32]. **b** Representative HAADF-STEM images of Pd/MWW catalyst formed under the reaction conditions for oxidative coupling of benzene. **c**–**f** Determination of the location of subnanometer Pd clusters in the Pd/MWW catalyst by HAADF-STEM and iDPC-STEM imaging technique. **c**, **e** HAADF-STEM images and **d**, **f** the paired iDPC-STEM images. **g**–**i** Scope study of the Pd/MWW catalyst for oxidative coupling of arenes.

partial pressure. The kinetic and isotopic studies indicate that Pd clusters confined in zeolites should follow a different reaction mechanism in comparison to the homogeneous Pd catalyst, and the rate-determining step on Pd clusters is probably the oxidation of O_2 rather than the C–H activation.

In liquid-phase oxidation reactions, H_2O can facilitate the adsorption and activation of O_2 at the metal active sites and, therefore, promote the catalytic performance in oxidation reactions, as reported with supported metal (Au, Pt, Pd, etc.) catalysts for oxidation of CO and alcohols[46–48]. The enhanced adsorption of O_2 on Pd clusters in the presence of H_2O is supported by the O_2-temperature programmed desorption profiles (Supplementary Fig. 86). It should be noted that the adsorption of H_2O on Pd clusters will not significantly modify their electronic properties according to the XPS and XANES characterization results (Supplementary Figs. 87, 88), implying that the co-adsorption of O_2 and water should lead to the formation of some activated oxygen species on the surface of Pd clusters.

One of the established mechanisms for O_2 activation with the assistance of H_2O involves the transfer of H from H_2O to O_2 for the production of •OOH and •OH species, as supported by the observation of promoted formation of active oxygen species (•OOH and •OH) in the electron spin resonance (ESR) spectra of the H_2O-promoted Pd/Na-Beta catalyst (Fig. 6d, e)[49]. Furthermore, due to the intense hydrogen bonding between H_2O and zeolite framework, the H transfer process could be hindered because of the lack of structural flexibility. By replacing H^+ with Na^+ to weaken the water–zeolite interaction, the H transfer process could be further facilitated, resulting in the greatly enhanced activity observed with the Pd/Na-Beta over the Pd/H-Beta catalyst.

Extending the substrate scope with Pd/MWW catalyst

The pore characteristics of Beta zeolite allow the regioselective production of 4,4′-bitolyl via the oxidative coupling of toluene. However, the small pore dimension of Beta zeolite (0.7–0.8 nm for the 12MR channels) also limits the substrate scope of the oxidative coupling between the benzene derivatives. The above characterization and mechanistic studies infer that the substrate scope could be extended by locating subnanometer Pd clusters in zeolite support with a larger cavity size. To validate this hypothesis, we have prepared a Pd/MWW catalyst by immobilizing subnanometer Pd clusters with sizes of 0.6–0.8 nm in the 12MR "surface cups" of MWW zeolite, as visualized in the HAADF-STEM and iDPC-STEM images (Supplementary Figs. 89–99). The 12MR surface cups serve as the anchoring sites for subnanometer Pd clusters and could provide a moderate confinement effect to influence the regioselective in the oxidative coupling reaction. For the oxidative coupling of benzene, the Pd/MWW catalysts also exhibit size-dependent catalytic performances and the Pd clusters with sizes of 0.5–0.6 nm show higher activity than the atomically dispersed Pd species and Pd clusters/nanoparticles with larger sizes (Supplementary Figs. 100–103).

We have tested a series of aromatics for the oxidative coupling reaction with the Pd/MWW catalyst. On the one hand, due to the absence of sufficient confinement effect, the Pd/MWW catalyst shows lower regioselectivity to 4,4′-bitolyl than the Pd/Beta catalysts. On the other hand, the Pd clusters in the Pd/MWW catalyst are more accessible to larger substrates than those in the Pd/Beta catalysts (Supplementary Fig. 104). As summarized in Fig. 7 and Supplementary Figs. 105–113, thanks to the improved accessibility of Pd clusters in the Pd/MWW catalyst, inter-molecular self-coupling of benzene derivatives larger than toluene and xylenes can be achieved (**2** and **3**), which is not feasible with Pd/Beta catalysts limited by their pore dimensions. Furthermore, the Pd/MWW catalyst can work for the intra-molecular coupling reactions for synthesizing dibenzofuran and Carbazole derivatives and the inter-molecular cross-coupling of large aromatic compounds (**4**–**9**). These results confirm the extensibility of the mechanistic insights on the working active sites in Pd-zeolite catalysts for oxidative coupling of aromatic compounds and the important role of the surrounding microenvironment of Pd clusters in controlling the reaction scope.

Discussion

Taking into account that metal-zeolite catalysts have great potential for numerous organic transformations, the structural transformation behaviour of the metal active sites under reaction conditions should be carefully studied to guide the catalyst's upgrading[50–52]. Furthermore, the microenvironment surrounding the metal active sites, formed by the zeolite framework and other molecules (solvent, ligand, reactant, product, etc.), could have significant impacts on the catalytic properties, which should be considered collectively for the design of supported metal catalysts for organic reactions.

Methods

Materials

Chemicals from commercial suppliers were used in experiments without further purification. Chemicals for the oxidative coupling of toluene: toluene (AR, Beijing Tongguang Co., Ltd.), palladium acetate ($Pd(OAc)_2$, >98%, Aldrich-Sigma), Beta zeolite (H-Beta, Si/Al ratio of 15, Nankai University catalyst Co. Ltd.), decane (≥99%, Aldrich-Sigma), Deuterium-substituted toluene (D8-Toluene Cambridge Isotope Laboratories Inc.), O_2 (99.9%, Beijing Huanyu Jinghui Capital Gas Technology Co., Ltd.) and $^{18}O_2$ (Wuhan Nionruide Special Gas Co., Ltd.). Chemicals for the synthesis of Na-Beta and Na-MWW zeolites: sodium hydroxide (analytic reagent, Shanghai Sinopharm Co., Ltd.), sodium aluminate ($NaAlO_2$, analytic reagent, Shanghai Macklin Biochemical Co. Ltd.), deionized water (Shanghai Titan Scientific Co., Ltd.), fumed silica (AEROSIL A200, Degussa), hexamethyleneimine (HMI, 98%, Alfa Aesar), sodium chloride (analytic reagent, Shanghai Sinopharm Co., Ltd.) and potassium chloride (analytic reagent, Shanghai Sinopharm Co., Ltd.).

Synthesis of Na-Beta samples

The Na-Beta samples were prepared by the ion exchange of commercial H-Beta with $NaHCO_3$. In a typical process, H-Beta zeolite (0.2 g) and a given amount of $NaHCO_3$ (1.25%, 2.5%, 3.75%, 6.25%, 10%, 25%, and 100% molar ratio relative to the amount of H^+ in H-Beta were dispersed/dissolved in deionized water (5 mL) and stirred at room temperature (RT) for 80 min. Na-exchanged Beta was subsequently isolated by centrifugation, washed once with 5 mL of deionized water, and dried at 60 °C for 12 h. Then, the dried sample was calcined in air at 500 °C for 2 h. The degree of ion exchange is determined by the mass ratio of H-Beta zeolite and $NaHCO_3$ and the resultant Na-Beta samples are named according to the relative amount of Na^+ with respect to the Al content in zeolite, which are derived from the ICP-OES analysis. For instance, in the 29Na-Beta sample, the amount of Na^+ is ~29% of the amount of Al in the pristine Beta zeolite.

Synthesis of Na-MWW zeolite

Na-MWW zeolite with a Si/Al ratio of 42 was synthesized in our laboratory through hydrothermal synthesis. $NaAlO_2$ (0.051 g), NaOH (0.078 g), NaCl (0.071 g), H_2O (16.47 g), HMI (1.16 mL) and 1.22 g SiO_2–A200 were mixed and stirred for 3 h. Subsequently, the mixture was moved into a Teflon-lined autoclave (50 mL) for hydrothermal crystallization at 135 °C under agitation conditions (60 rpm) for 7 days. Following the hydrothermal crystallization process, the solids were obtained by centrifugation and washed with acetone and water. After that, Na-MWW zeolites were obtained by the calcination of dried solids in the air at 560 °C for 8 h.

Synthesis of Pd/MWW zeolite

MWW zeolite-supported Pd catalyst was synthesized by mixing the zeolite and $Pd(OAc)_2$ in toluene. In a typical preparation, toluene (4 mL), $Pd(OAc)_2$ (15 μmol) and Na-MWW zeolite (40 mg) were mixed to form a suspension in an autoclave. The autoclave reactor was pressurized with 16 bar of O_2 and then maintained at 110 °C for 1 h with stirring. Once cooled to RT, the Pd/MWW zeolite was separated and then dried in a fuming cupboard overnight.

Characterizations

Matrix-assisted laser desorption/ionization coupled to time-of-flight (MALDI-TOF) measurements were conducted using a MALDI SYNAPT G2-Si HDMS (Waters, Wilmslow, UK) mass spectrometry instrument. Before the measurements, the reaction mixture (20 μL) was diluted in 1 mL of acetonitrile. The UV–vis light fluorescence spectra were performed using a fluorescence spectrometer (UV-800C, HORIBA, USA). Before the UV–vis measurements, the Pd-containing solution was diluted to a Pd concentration of ~0.35 mmol/L in toluene. Powder X-ray diffraction (XRD) patterns were conducted using a Rigaku RU-200b X-ray powder diffractometer (Cu Kα). X-ray photoelectron spectroscopy (XPS) measurements were carried out on a Thermo ESCALAB 250XI electron spectrometer using monochromatic Al Kα radiation. Regarding the quasi-in situ XPS, the sample was treated with water vapour produced by the bubble along with helium at atmosphere pressure (20 mL/min), and then the sample was moved to the analysis chamber. The Pd and Na contents of samples were obtained by inductively coupled plasma optical emission spectroscopy (ICP-OES) with the PerkinElmer Optima 2100DV. The acidic properties of catalysts were ascertained by means of pyridine-adsorbed infra-red (Py-IR) spectra obtained using a Thermo scientific spectrometer (Nicolet iS50). The water vapour adsorption–desorption measurement was performed in a Dynamic Vapour Sorption (3H-2000PW, Beijing

Beishide Instrument Technology Co., Ltd). Temperature-programmed desorption of oxygen (O_2-TPD) was conducted with an Autosorb-iQ-C chemisorption analyser (Quantachrome, USA). Typically, the sample was activated at 473 K in argon flow (30 mL/min) for 1 h. Before the desorption, The sample was maintained at 323 K in an O_2 atmosphere (30 mL/min) for 30 min. Subsequently, it was purged by a flow of argon (30 mL/min) for 1 h. The desorption process was measured by a TCD when heating the sample from 323 to 1073 K in helium flow (30 mL/min).

For the measurements by electron microscopes, the samples were dispersed in a dichloromethane and then dropped onto copper meshes covered by ultra-thin carbon films. Low-resolution HAADF-STEM images were collected by the JEOL 2100F microscope. Aberration-correct HAADF-STEM and paired iDPC-STEM images were recorded with an FEI Titan Themis Z microscope.

The ex-situ X-ray absorption experiments (XAS) were conducted at the Spring-8 synchrotron facility. Data analysis and EXAFS fitting were done with Athena and Artemis programmes of the Demeter data analysis packages using FEFF6 programme[53,54]. Energy calibration was conducted via a standard Pd foil measured simultaneously. After applying a Hanning window function ($\Delta k = 1.0$), the k^3-weighted $\chi(k)$ data were subjected to Fourier transformation. For EXAFS modelling, the global amplitude EXAFS (CN, R, σ^2 and $\Delta E0$) were obtained through nonlinear fitting in R-space with Artemis software. The EXAFS of Pd foil was fitted, and the $S0^2$ value (0.944) was set to determine the coordination numbers of Pd–O and Pd–Pd in the sample. The in situ XANES measurement was performed at the ALBA synchrotron light source. In a typical experiment, the Pd/29Na-Beta-1h sample was placed into a capillary, then helium saturated with water vapour at atmosphere pressure was introduced at a total gas flow rate of 10 mL/min, and the XANES spectra were collected at 110 °C at various times.

The attenuated total reflectance infrared spectra (ATR-IR) of adsorbed H_2O on H-Beta and 29Na-Beta samples were recorded at 50 °C with a Fourier-transformed IR (FT-IR) spectrometer using an MCT detector (1 cm^{-1}). For a typical ATR-IR study, the sample (~30 mg) was dispersed in 1 mL CH_3CN and then coated on a ZnSe cylindrical internal reflection element (IRE). The IRE with catalyst was placed in an ATR flow cell, which was fixed on an FT-IR spectrometer (Perkin Elmer, Fourier). The sample was pre-treated at 150 °C in flowing He (10 μL/min) for 2 h to remove CH_3CN and any other adsorbed impurities. Then, background spectra were collected in helium flow at 30 °C. Subsequently, helium saturated with water vapour at atmosphere pressure was introduced (50 mL/min), and the IR spectra were collected at 50 °C.

^{1}H-MAS solid-state NMR experiments were conducted on a JNM-ECZ600R 600 MHz NMR spectrometer with a tube diameter of 3.2 nm at room temperature. In particular, H-Beta and 29Na-Beta samples (0.2 g) were degassed at room temperature and further dried at 150 °C in the helium flow (50 mL/min) for 2 h. Subsequently, 20 μL of H_2O was introduced to the zeolite samples at 60 °C. The samples were then quickly transferred into the NMR tube to initiate the test. EPR spectra were collected at RT using the Bruker A300. 5,5-Dimethyl-1-pyrroline N-oxide (DMPO) was used as the spin-trapping agent for monitoring reactive species such as ·OOH and ·OH radicals. For ·OOH radical detection, 20 mg of Pd/29Na-Beta-1h were degassed at room temperature and then dispersed in 2 mL of toluene (20 μL H_2O was included for H_2O-involved testing) by ultrasound, followed by the introduction of O_2 at a flow rate of 50 mL/min for 10 min. Subsequently, 200 μL of the mixed solution was added to 100 μL of a 100 mmol/L DMPO–methanol solution. The final mixture was transferred into a capillary tube for testing. The procedure for the detection of ·OH radicals is the same as that for the detection of ·OOH radicals, with the only difference being the replacement of the 100 mmol/L DMPO–methanol solution with a 100 mM aqueous DMPO solution. ^{1}H NMR of products was carried on a Bruker AVANCE III HD 400M spectrometer, and deuterated DMSO or $CHCl_3$ was used as a solvent.

Simulation of HAADF-STEM images

The simulations of high-resolution HAADF-STEM images were conducted using the TEMSIM software[55]. The optoelectronic parameters for simulations are based on the electron microscope settings in this work: HT = 300 kV, Cs5 = 5 mm, Cs3 = −0.001 mm, convergence angle = 18 mrad, detector size = 68–200 and 49–200 mrad. For practical images, final simulations are convolved with a Gauss blur filter in MATLAB. Complex structural models for simulations are constructed with Rhodius software from Cadiz University[56].

Catalytic tests

The oxidative coupling of toluene is performed in high-pressure autoclave reactors. Typically, toluene (4 mL), $Pd(OAc)_2$ (15 μmol), and Beta zeolite (50 mg) were added into a glass-lined autoclave (12 mL), which was sealed and purged with O_2 three times. The reactor was pressurized with O_2 (16 bar) and placed in an oil bath at 110 °C. The pressure at 110 °C was maintained at 20 bar. After the reaction time, decane (200 μL, used as an internal standard) was added, and the liquid was diluted with toluene for analysis by gas chromatography (GC) (Agilent 6890) equipped with a flame ionization detector using N_2 as the carrier gas. The column was a 30 m × 0.32 mm HP-5 (Agilent) with a film thickness of 0.25 μm. The turnover numbers of the converted toluene molecules were calculated by normalizing the converted amount of toluene to the number of Pd atoms added to the reaction mixture.

Data availability

The data that support the findings of this study are available in the article and its Supplementary Information. All data are available from the authors upon request.

References

1. Corma, A. Heterogeneous catalysis: understanding for designing, and designing for applications. *Angew. Chem. Int. Ed.* **55**, 6112–6113 (2016).
2. Ellis, P. J., Fairlamb, I. J. S., Hackett, S. F. J., Wilson, K. & Lee, A. F. Evidence for the surface-catalyzed Suzuki–Miyaura reaction over palladium nanoparticles: an operando XAS study. *Angew. Chem. Int. Ed.* **49**, 1820–1824 (2010).
3. Kashin, A. S. & Ananikov, V. P. Catalytic C–C and C–heteroatom bond formation reactions: in situ generated or preformed catalysts? Complicated mechanistic picture behind well-known experimental procedures. *J. Org. Chem.* **78**, 11117–11125 (2013).
4. Eremin, D. B. & Ananikov, V. P. Understanding active species in catalytic transformations: from molecular catalysis to nanoparticles, leaching, "Cocktails" of catalysts and dynamic systems. *Coord. Chem. Rev.* **346**, 2–19 (2017).
5. Martín, A. J., Mitchell, S., Mondelli, C., Jaydev, S. & Pérez-Ramírez, J. Unifying views on catalyst deactivation. *Nat. Catal.* **5**, 854–866 (2022).
6. Buurmans, I. L. C. & Weckhuysen, B. M. Heterogeneities of individual catalyst particles in space and time as monitored by spectroscopy. *Nat. Chem.* **4**, 873–886 (2012).
7. Costa, P., Sandrin, D. & Scaiano, J. C. Real-time fluorescence imaging of a heterogeneously catalysed Suzuki–Miyaura reaction. *Nat. Catal.* **3**, 427–437 (2020).
8. Malta, G. et al. Identification of single-site gold catalysis in acetylene hydrochlorination. *Science* **355**, 1399–1403 (2017).
9. Chee, S. W., Arce-Ramos, J. M., Li, W., Genest, A. & Mirsaidov, U. Structural changes in noble metal nanoparticles during CO oxidation and their impact on catalyst activity. *Nat. Commun.* **11**, 2133 (2020).
10. Vogt, E. T. C. & Weckhuysen, B. M. Fluid catalytic cracking: recent developments on the grand old lady of zeolite catalysis. *Chem. Soc. Rev.* **44**, 7342–7370 (2015).

11. Li, X., Wang, X., Roy, K., van Bokhoven, J. A. & Artiglia, L. Role of water on the structure of palladium for complete oxidation of methane. *ACS Catal.* **10**, 5783–5792 (2020).
12. Goodman, E. D. et al. Catalyst deactivation via decomposition into single atoms and the role of metal loading. *Nat. Catal.* **2**, 748–755 (2019).
13. Liu, L. & Corma, A. Evolution of isolated atoms and clusters in catalysis. *Trends Chem.* **2**, 383–400 (2020).
14. Collis, A. E. C. & Horváth, I. T. Heterogenization of homogeneous catalytic systems. *Catal. Sci. Technol.* **1**, 912–919 (2011).
15. Ye, R., Zhukhovitskiy, A. V., Deraedt, C. V., Toste, F. D. & Somorjai, G. A. Supported dendrimer-encapsulated metal clusters: toward heterogenizing homogeneous catalysts. *Acc. Chem. Res.* **50**, 1894–1901 (2017).
16. Grzybowski, M., Sadowski, B., Butenschön, H. & Gryko, D. T. Synthetic applications of oxidative aromatic coupling—from biphenols to nanographenes. *Angew. Chem. Int. Ed.* **59**, 2998–3027 (2019).
17. Vercammen, J. et al. Shape-selective C–H activation of aromatics to biarylic compounds using molecular palladium in zeolites. *Nat. Catal.* **3**, 1002–1009 (2020).
18. Van Velthoven, N. et al. Single-site metal-organic framework catalysts for the oxidative coupling of arenes via C–H/C–H activation. *Chem. Sci.* **10**, 3616–3622 (2019).
19. Wang, D., Izawa, Y. & Stahl, S. S. Pd-catalyzed aerobic oxidative coupling of arenes: evidence for transmetalation between two Pd(II)-Aryl intermediates. *J. Am. Chem. Soc.* **136**, 9914–9917 (2014).
20. Wen, W. et al. Fluorescent PEI@Pd nanoclusters: facile synthesis and application. *RSC Adv.* **11**, 33202–33207 (2021).
21. Leyva-Perez, A., Oliver-Meseguer, J., Rubio-Marques, P. & Corma, A. Water-stabilized three- and four-atom palladium clusters as highly active catalytic species in ligand-free C–C cross-coupling reactions. *Angew. Chem. Int. Ed. Engl.* **52**, 11554–11559 (2013).
22. Pun, D., Diao, T. & Stahl, S. S. Aerobic dehydrogenation of cyclohexanone to phenol catalyzed by Pd(TFA)2/2-dimethylaminopyridine: evidence for the role of Pd nanoparticles. *J. Am. Chem. Soc.* **135**, 8213–8221 (2013).
23. Phan, N. T. S., Van Der Sluys, M. & Jones, C. W. On the nature of the active species in palladium catalyzed Mizoroki–Heck and Suzuki–Miyaura couplings—homogeneous or heterogeneous catalysis, a critical review. *Adv. Synth. Catal.* **348**, 609–679 (2006).
24. Sherwood, J., Clark, J. H., Fairlam, I. J. S. & Slattery, J. M. Solvent effects in palladium catalysed cross-coupling reactions. *Green Chem.* **21**, 2164–2213 (2019).
25. Unger, M. O. & Fouty, R. A. Oxidative coupling of toluene through organometallic intermediates. *J. Org. Chem.* **34**, 18–21 (2002).
26. van Benthem, R. A. T. M., Hiemstra, H., van Leeuwen, P. W. N. M., Geus, J. W. & Speckamp, W. N. Sulfoxide-stabilized giant palladium clusters in catalyzed oxidations. *Angew. Chem. Int. Ed. Engl.* **34**, 457–460 (2003).
27. Zhang, Y., Enomoto, Y. & Iwata, T. Synthesis and characterization of biphenyl polyesters derived from divanillic acid and cyclic diols. *Polymer* **203**, 122751 (2020).
28. Liu, L., Lopez-Haro, M., Calvino, J. J. & Corma, A. Tutorial: structural characterization of isolated metal atoms and subnanometric metal clusters in zeolites. *Nat. Protoc.* **16**, 1871–1906 (2020).
29. Okumura, K. et al. Energy-dispersive XAFS studies on the spontaneous dispersion of PdO and the formation of stable Pd clusters in zeolites. *J. Phys. Chem. B* **108**, 6250–6255 (2004).
30. Li, T. et al. Stable palladium oxide clusters encapsulated in silicalite-1 for complete methane oxidation. *ACS Catal.* **11**, 7371–7382 (2021).
31. Boucly, A. et al. Water inhibition and role of palladium adatoms on Pd/Al_2O_3 catalysts during methane oxidation. *Appl. Surf. Sci.* **606**, 154927 (2022).
32. Baerlocher, Ch, McCusker, L. B., Gies, H. & Marler, B. *Database of Disordered Zeolite Structures* http://www.iza-structure.org/databases/ (2017).
33. Liu, L. et al. Regioselective generation and reactivity control of subnanometric platinum clusters in zeolites for high-temperature catalysis. *Nat. Mater.* **18**, 866–873 (2019).
34. Wang, N. et al. In situ confinement of ultrasmall Pd clusters within nanosized silicalite-1 zeolite for highly efficient catalysis of hydrogen generation. *J. Am. Chem. Soc.* **138**, 7484–7487 (2016).
35. Zhang, F. et al. Selective hydrogenation of CO_2 to ethanol over sodium-modified rhodium nanoparticles embedded in zeolite silicalite-1. *J. Phys. Chem. C* **125**, 24429–24439 (2021).
36. Petrov, A. W. et al. Stable complete methane oxidation over palladium based zeolite catalysts. *Nat. Commun.* **9**, 2545 (2018).
37. Gao, D., Wang, S., Zhang, C., Yuan, Z. & Wang, S. Methane combustion over Pd/Al_2O_3 catalyst: effects of chlorine ions and water on catalytic activity. *Chin. J. Catal.* **29**, 1221–1225 (2008).
38. Wilson, N. M. & Flaherty, D. W. Mechanism for the direct synthesis of H_2O_2 on Pd clusters: heterolytic reaction pathways at the liquid–solid interface. *J. Am. Chem. Soc.* **138**, 574–586 (2015).
39. Persson, K., Pfefferle, L. D., Schwartz, W., Ersson, A. & Järås, S. G. Stability of palladium-based catalysts during catalytic combustion of methane: the influence of water. *Appl. Catal. B: Environ.* **74**, 242–250 (2007).
40. Stanciakova, K. & Weckhuysen, B. M. Water–active site interactions in zeolites and their relevance in catalysis. *Trends Chem.* **3**, 456–468 (2021).
41. Wang, Y. et al. The study of Pd-SSZ-13 as low-temperature passive NO adsorber materials: high dispersal of Pd in small-pore CHA zeolites by thermal treatment. *Appl. Catal. B: Environ.* **324**, 122254 (2023).
42. Bakker, H. J. & Skinner, J. L. Vibrational spectroscopy as a probe of structure and dynamics in liquid water. *Chem. Rev.* **110**, 1498–1517 (2010).
43. Shelyapina, M. G. et al. Nanoconfined water in pillared zeolites probed by ^{1}H nuclear magnetic resonance. *Int. J. Mol. Sci.* **24**, 15898 (2023).
44. Li, S. et al. Extra-framework aluminium species in hydrated faujasite zeolite as investigated by two-dimensional solid-state NMR spectroscopy and theoretical calculations. *Phys. Chem. Chem. Phys.* **12**, 3895–3903 (2010).
45. Crupi, V., Longo, F., Majolino, D. & Venuti, V. Vibrational properties of water molecules adsorbed in different zeolitic frameworks. *J. Phys.: Condens. Matter* **18**, 3563–3580 (2006).
46. Zope, B. N., Hibbitts, D. D., Neurock, M. & Davis, R. J. Reactivity of the gold/water interface during selective oxidation catalysis. *Science* **330**, 74–78 (2010).
47. Saavedra, J., Doan, H. A., Pursell, C. J., Grabow, L. C. & Chandler, B. D. The critical role of water at the gold–titania interface in catalytic CO oxidation. *Science* **345**, 1599–1602 (2014).
48. Wei, Q. et al. Recognition of water-induced effects toward enhanced interaction between catalyst and reactant in alcohol oxidation. *J. Am. Chem. Soc.* **143**, 6071–6078 (2021).
49. Jeong, M. S. et al. Methodological considerations of electron spin resonance spin trapping techniques for measuring reactive oxygen species generated from metal oxide nanomaterials. *Sci. Rep.* **6**, 26347 (2016).
50. Mon, M. & Leyva-Pérez, A. Zeolites catalyze selective reactions of large organic molecules. *Adv. Catal.* **69**, 59–102 (2021).
51. Djakovitch, L. & Koehler, K. Heck reaction catalyzed by Pd-modified zeolites. *J. Am. Chem. Soc.* **123**, 5990–5999 (2001).
52. Garnes-Portolés, F. et al. Regioirregular and catalytic Mizoroki–Heck reactions. *Nat. Catal.* **4**, 293–303 (2021).

53. Ravel, B. & Newville, M. ATHENA,ARTEMIS,HEPHAESTUS: data analysis for X-ray absorption spectroscopy usingIFEFFIT. *J. Synchrotron Radiat.* **12**, 537–541 (2005).
54. Zabinsky, S. I., Rehr, J. J., Ankudinov, A., Albers, R. C. & Eller, M. J. Multiple-scattering calculations of x-ray-absorption spectra. *Phys. Rev. B* **52**, 2995–3009 (1995).
55. Kirkland, E. J. *Advanced Computing in Electron Microscopy* (Springer, 2010).
56. Bernal, S. et al. The interpretation of HREM images of supported metal catalysts using image simulation: profile view images. *Ultramicroscopy* **72**, 135–164 (1998).

Acknowledgements

Financial support from the National Natural Science Foundation of China (No. 22272087, L.L.), China Postdoctoral Science Foundation (No. 2022M721806, Y.F.) and Tsinghua University (Initiative Scientific Research Programme (20233080016, L.L.), Tsinghua-Jiangyin Innovation Special Fund (TJISF, 20222000555, L.L.) and Dushi Programme (20231080010, L.L.)) are greatly acknowledged. We also greatly appreciate SINOPEC's support through the SEED project on our project. B.T.W.L. thanks the support from the National Natural Science Foundation of China (No. 22172136) and Hong Kong Research Grants Council (15301521 and 15305722). M.L.-H. thanks to the financial support from PID2022-142312NB-I00 funding by MCIN/AEI/10.13039/50110001103. The in situ XANES experiments were performed at the NOTOS BL16 beamline at ALBA Synchrotron with the collaboration of ALBA staff.

Author contributions

L.L. conceived the project, directed the study and wrote the manuscript. Y.F. carried out the synthesis, structural characterizations, and catalytic tests and contributed to the preparation of the manuscript. H.W. contributed to the synthesis of zeolite materials. T.C. and B.T.-W.L. analysed the XAS data. F.H., Z.H. and C.M. contributed to the collection of the in situ XANES data at the ALBA synchrotron. M.L.H. did the simulation of the HAADF-STEM images of Pd-zeolite catalysts. All the authors discussed the results and contributed to the formation of the manuscript.

Competing interests

The authors declare no competing interests.

Additional information

Supplementary information The online version contains supplementary material available at https://doi.org/10.1038/s41467-024-53475-z.

Correspondence and requests for materials should be addressed to Lichen Liu.

Peer review information *Nature Communications* thanks the anonymous reviewers for their contribution to the peer review of this work. A peer review file is available.